Proceedings of the 10th International Conference on Fluid Flow, Heat and Mass Transfer (FFHMT'23)
Canada – June 07-09, 2023
Paper No. 131
DOI: 10.11159/ffhmt23.131

Effect of Location of Rectangular Orifice on the Momentum flow of Power-law Fluids

Anamika Maurya[1], Rajendra Chhabra[2]
[1]School of Engineering and Applied Science, Ahmedabad University
Navrangpura, Ahmedabad, 380009, Gujrat, INDIA
[2]Department of Chemical Engineering, School of Engineering, Shiv Nadar University
Dadri, Greater Noida, Delhi, 201314, India
anamika.maurya@ahduni.edu.in; rajendra.chhabra@snu.edu.in

Abstract **–** The present work numerically investigates the flow of power-law fluids through a square-edged rectangular orifice. This study has been carried out for a wide range of power-law index (0.3 – 1.0) and three lateral positions of the orifice (0.5 – 0.75) at a fixed Reynolds number (i.e., 20) and aspect ratio (i.e., 0.5). This work aims to understand the influence of the shift of the location of the orifice in the lateral direction on the flow characteristics. The new results have been presented in this work in the form of flow patterns, central and lateral velocity profiles, and the discharge coefficient. Notably, the flow pattern demonstrates the formation of symmetric and antisymmetric flow separation zones in the vicinity of the orifice, depending upon the orifice location, regardless of the power-law index. In this work, an effort has been made to analytically derive the equation for the discharge coefficient of non-Newtonian fluids through the rectangular channel and presented the same for a wide range of conditions. Results demonstrate that the flow velocities, i.e., centreline and lateral velocity profiles are a strong function of the governing parameters and orifice location. The discharge coefficient is seen as an increasing function of the orifice location as it shifts in the lateral direction, towards the upper wall of the computational domain. Also, a dramatic effect of the power-law index on the discharge coefficient has been observed herein for a particular orifice location.

Keywords**:** rectangular orifice, orifice location, flow characteristic, power-law fluids, discharge coefficient, separation zones

1. Introduction

In the past several decades, worldwide, in the process industries, for instance, oil, chemical, energy, pharmaceuticals, food, etc., the flow generally occurs through a channel/container/pipe/industrial tank, etc. In processing fluids from such industrial configurations, it has been learned through the industries that discharging the working fluids through the industrial settings is a reasonably complex problem in transport phenomena. It has been experienced from the industries that a controlled, accurate, and efficient measurement of the flow rates/discharge coefficient of the working fluids, either Newtonian [1 -2] or non-Newtonian [3] (for instance, power-law fluids, Bingham plastic fluids, Hershel Bulkley fluids, etc.) is in demand. In particular, this work aims to discuss numerically the flow characteristics of the non-Newtonian fluids, which are being considered in industries such as personal care, food, etc. For flow measurements, one of the typical flow meters used in the process industries is the orifice meter [1-3]. However, for the orifice meters, a high pumping cost has been noted by the engineers due to the higher pressure losses; still, it remains the choice of at least 40% of industries in use because of its ruggedness. Literature covers numerous studies investigating Newtonian fluids flow such as air/water through an orifice, but the information regarding non-Newtonian fluids is scarce. Thus, predicting the flow of non-Newtonian fluids through the orifices remains an active area of research. Some additional advantages of using the orifice as a flow meter can be found in References [4-6]. Also, the orifice is preferred in the industries basis on its simple working principal, which is based on the pressure drop due to contraction/expansion in its vicinity. It is a kind of differential-pressure-based flow measurement device used in industries. Thus, the present work aims to explore the flow of non-Newtonian fluids through the rectangular orifice meter for a wide range of conditions.

2. Literature Review and Objectives

Literature is rich with experimental and numerical work detailing the discharge of Newtonian [1–2, 4-5] and non-Newtonian fluids [7-11]. However, through rigorous literature review, it has been noted that most of the literature related to the orifice is dedicated to the turbulence flows, which supports several realistic conditions; hence the flow discharge coefficient is generally thought about as constant. But, with several industrial applications, it has been learned that the laminar flow through an orifice is also essential. It is being considered in industries as it represents a functional relationship with the

Reynolds number, the shape of the orifice, the location of the orifice, etc. The result predicted from such analysis is being utilized in the industries as a precursor to predicting the flow rate, which is the focus of the present work [12]. A few exciting review articles based on the flow of Newtonian and non-Newtonian fluids through an orifice have been recently added to the literature [13 - 15]. However, a few works of literature directly related to non-Newtonian fluids have been discussed in this work to confirm the novelty of the present work.

Ntamba and Fester [7] experimentally observed the pressure loss coefficient for the flow of Newtonian and non-Newtonian fluids (i.e., Kaolin, CMC, and Bentonite) through a short square-edged orifice plate for a wide range of conditions as $5 \leq Re \leq 106$, $0.2 \leq \beta \leq 0.7$; $0.3 \leq n \leq 1$. They worked in the flow regimes as laminar, transitional, and turbulent using Hershel Bulkley fluids. They discussed the industrial importance of such loss coefficients in piping systems. However, in this work, they discussed the importance of laminar flow through short orifices at low Reynolds numbers. Importantly, they defined a limiting value of the Reynolds number, i.e., the same for all fluid and aspect ratios to demarcate the pure laminar and pure turbulent flow regimes. Later, this work has also been expanded by Chowdhury and Fester [8] for the power-law, Hershel Bulkley, and Newtonian fluids for a long sharp-edged orifice. Further, Khahledi et al. [9] experimentally observed the flow rate measurement of non-Newtonian fluids, i.e., aqueous CMC solution and water-based suspension of kaolin and bentonite through a sharp crested notch, mainly rectangular and V-shaped. They predicted the laminar flow relationship between the discharge coefficient and Reynolds number with the help of a single composite equation for such a system. They also specified the range of the Reynolds number for transition and turbulent flows. Subsequently, Rituraj and Vacca [10] conducted both the experimental and numerical investigation of the flow of non-Newtonian fluid through a sharp orifice with a small aperture in the laminar regime for a wide range of conditions. This work highlighted the importance of sharp orifices of lower diameters ratios in the process industries. However, they limited their work to $\beta < 0.2$, i.e., generally encountered in dishwashing liquid bottles. Recently, Khahledi et al. [11] extended their work to observe the discharge of both Newtonian and non-Newtonian fluids from a rectangular tank through three different shapes of the orifice as circular, square and triangular for a wide range of conditions as $0.02 \leq \beta \leq 0.05$; $0.10 \leq Re \leq 105$, $0.36 \leq n \leq 1$. In this work, they have developed a discharge coefficient versus Reynolds number relationship that can be utilized in process engineering and design for flow measurement through sharp crested orifices.

Basis, the above literature survey, it can be noted that though several studies have been done in the field of the flow of complex fluids through an orifice, still, the information related to the laminar and incompressible flow of power-law and Newtonian fluids through a rectangular shaped orifice is limited in terms of shift of the location of the orifice in the channel. Therefore, the present work aims to fill this gap in the body of knowledge. The current work aims to investigate numerically the flow characteristics of the power-law ($n < 1$) and Newtonian fluids ($n = 1$) flowing through a rectangular-shaped orifice fitted in a rectangular channel having the aspect ratio as $\beta = 0.5$. This work explores the orifice location (i.e., Co) at different positions in the lateral direction to the flow field, i.e., 0.5, 0.65, and 0.75. A detailed discussion on the influence of the input/governing parameters on the flow fields have been done in this work through numerical simulations.

3. Problem Description and Numerical Strategy

Figure 1 represents the computational domain, boundary conditions, coordinate systems, etc., for the present work. An incompressible power-law fluid with a fully developed velocity profile enters through the inlet plane. The average velocity of the fluid has been taken as Uo. The fluid has experienced a sudden contraction and expansion due to the fitted rectangular-shaped orifice in the flow domain. Such configuration of the computational domain leads to the modulation in the flow and pressure fields, and hence a boundary layer separation occurs. The present numerical model assumes the flow to be two-dimensional, steady, and incompressible. Also, the current work has been carried out in the forced convective regime and does not exploit the body forces herein. However, in the inertial frame of reference, the fluid dynamics (by continuity and momentum) of the present work are governed by the following non-dimensional equations [16-17]:

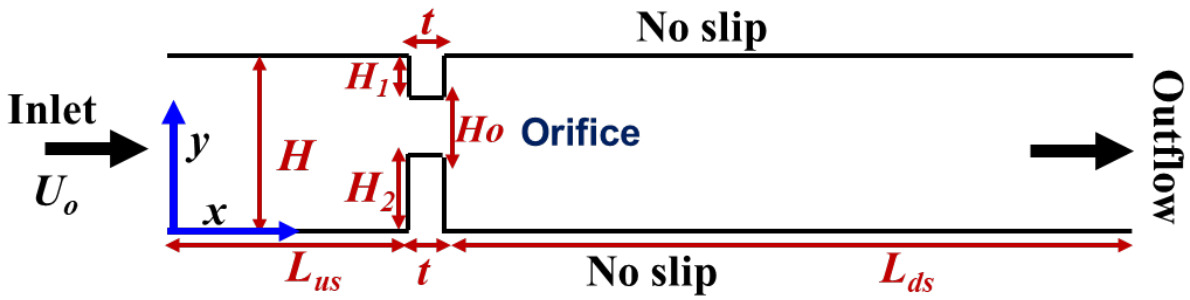

Fig. 1. Schematic representation of the computational domain and boundary conditions.

Continuity equation: $\nabla \cdot U = 0$ (1)

Momentum equation: $(U \cdot \nabla)U = -\nabla P + \frac{1}{Re}\nabla \cdot \tau$ (2)

In this work, the average velocity of the working fluid, U_o, has been used as the velocity scale, and the width of the channel, H, has been used as the length scale. In the above Eqns. (1) and (2), U is the non-dimensional velocity field, which has been scaled by U_o. Further, U_x and U_y are the velocity components in the x- and y-directions. Also, P represents a non-dimensional pressure scaled by ρU_o^2. The shear stress, τ shown in Eqn. (2) has been non-dimensionalised by $m(U_o/H)^n$, where "m" is the power-law fluid consistency index. Notably, the symbol Re demonstrates the usual dimensionless parameters as Reynolds number.

Along with the above model Eqns. (1) – (2), the numerical simulation has been carried out in conjunction with the extra stress tensor in regards to the working fluids, defined as [16-17]:

$$\tau = 2\,\eta(\dot{\gamma})\boldsymbol{D} \quad \text{where} \quad \boldsymbol{D} = \frac{1}{2}\left[\nabla U + (\nabla U)^T\right] \tag{3}$$

where η, $\dot{\gamma}$ and $\boldsymbol{D}$ are the apparent fluid viscosity, the rate of the strain tensor, and the symmetric part of the velocity gradient of the flow field, respectively.

The scalar viscosity function $\eta(\dot{\gamma})$ for the power-law fluids is defined as follows [16-17]:

$$\eta = \left(\frac{I_2}{2}\right)^{\left(\frac{n-1}{2}\right)} \text{ and } I_2 = \sum_i \sum_j \dot{\gamma}_{ij}.\dot{\gamma}_{ji} \text{ where } (i,j) = (r,z) \tag{4}$$

However, the above model Eqns. (1) – (4) has been solved using the following boundary conditions in this work as:

At Inlet: $U_x = \left(\frac{2n+1}{n+1}\right)\left[1-\left(\left|1-\frac{y}{H}\right|\right)^{n+1/n}\right]$, $U_y = 0$, $0 \le y \le H$

At Outlet: $\frac{\partial \phi}{\partial N} = 0$; where ϕ is dependent variable as $\boldsymbol{U}$; N is the unit normal

At channel and orifice walls: $U_x = 0$; $U_y = 0$

The present work has four non-dimensional parameters: Reynolds number, Re, power-law index, n, aspect ratio, β, and orifice location as Co (normalized by H). A few of them have been defined as follows:

- $Re = \frac{\rho H^n U_o^{2-n}}{m}$ (5)
- $\beta = \left(\frac{H_o}{H}\right)$ (6)

This work has been carried out for a fixed value of Reynolds number, i.e., $Re = 20$, ensuring the flow field to be steady and laminar. Further, a wide range of power-law index has been taken herein, which provides the coverage of highly shear-thinning fluids (i.e., $n = 0.3$) to Newtonian fluids (i.e., $n = 1$). Furthermore, three different values of C_o have been taken in this work as 0.5, 0.65, and 0.75. Such values demonstrate the three different locations of the orifice in the rectangular channel as $C_o = 0.5$ coincides with the centre of the orifice with the channel cross-section, i.e., at $Y = 0.5$; for $C_o = 0.65$, the centre of the orifice will be placed at $Y = 0.65$ (i.e., a location in between the channel centre and upper wall). Similarly, for $C_o = 0.75$, the centre of the orifice will be at $Y = 0.75$ (i.e., close to the upper channel wall).

To ensure the fully developed flow in the flow domain, a sufficiently long upstream length, i.e., L_{us} and downstream length, L_{ds} have been chosen herein., see Fig. 1. For the present work, grid sensitivity analysis has been carried out using three different grid resolutions as 124121, 254052, 434542 with the mapped grid structure with fine grids close to the channel walls to capture the gradient appropriately (details has not been shared for the conciseness of the paper). However, basis the velocity and pressure profiles, the grid points as 254052 have been considered in this work to ensure the numerical accuracy of the results. Further, this work used the convergence criterion as 10^{-6}. All the governing equations and the boundary conditions, has been solved using finite-element-based software COMSOL Multiphysics [16-17]. It is important to mention herein that to ensure the accuracy and reliability of the present numerical scheme, the numerical solution procedure has been validated with the available related literatures with ± 5.5% deviation [16-17].

4. Results and Discussion

4.1. Streamline Patterns

Figures 2 and 3 represent the typical streamline patterns for highly shear-thinning and Newtonian fluids, respectively for a fixed Reynolds number, i.e., $Re = 20$, and aspect ratio, i.e., $\beta = 0.5$ for three different lateral positions of orifice, i.e., $C_o = 0.5$ (represents the centre of the orifice at $Y = 0.5$), 0.65 (represents the centre of the orifice at $Y = 0.65$) and 0.75 (represents the centre of the orifice at $Y = 0.75$). It is interesting to note that the streamline patterns in the vicinity of the obstruction region are seen to be significantly affected by the positioning of the orifice in the lateral direction, regardless of the fluids, i.e., shear-thinning and Newtonian, see Figs. 2 and 3. Notably, a distortion in the streamline pattern has been observed close to the obstruction region as the fluid experiences a sudden expansion in the flow direction [17]. Such experience leads to cause an adverse pressure gradient resulting in the separation zones [16-17]. Along with positioning of the orifice in the lateral direction, such separation zones show a substantial dependency on the type of fluids studied in this work. It is worth mentioning herein that the two separation zones have been observed for the case of $C_o = 0.5$ and 0.65, see Fig. 2(a) and (b); and Fig. 3(a) and (b). On the other hand, for $C_o = 0.75$, only one separation zone has been observed in the computational domain, which is at the lower wall of the channel, Figs. 2(c) and 3(c). In particular, for $C_o = 0.5$, a symmetric flow separation zones, i.e., at the lower and upper walls of the channel, separation length, $L_r = 1.48$, see Fig.2(a), can be seen for either highly shear thinning fluids (see, Fig. 2a) or Newtonian fluids (see, Fig. 3a). On the other hand, for the orifice location of $C_o = 0.65$, asymmetric separation zones have been observed close to the upper and lower walls in the vicinity of constraint region. Interestingly, the separation zone close to the channel upper wall is significantly smaller ($L_r = 0.254$) than the separation zones at the lower wall ($L_r = 2.51$), see Fig. 2(b). Moreover, for $C_o = 0.75$, only one separation zone has been observed at the lower wall of the channel with $L_r = 3.30$, see Fig. 2(c) as also discussed above. For the monitoring of the separation zones, our previous research article can be referred [16-17], see Fig. 2(a).

From Fig. 3, for the Newtonian fluids, i.e., $n = 1.0$, the distortion in the form of symmetry and asymmetry in the flow field has been seen to be almost similar to Fig. 2. However, the separation zone length, L_r for the Newtonian fluids is found to be significantly smaller than the highly shear-thinning fluids, $n = 0.3$ (Fig. 2). Importantly, for the shear-thinning fluids ($n \leq 1$), no separation zones have been observed in the upstream region regardless of the orifice positioning and studied parameters. On the other hand, for the Newtonian fluids, separation zones, though feeble, have been noted in the upstream region of the orifice for all C_o. This is due to the reason that the Newtonian fluids are viscous than the shear-thinning fluids and offer more resistance to movement, and hence get sticks to the corners in the upstream region of the channel. On the other hand, the shear-thinning fluids ($n \leq 1$), being less viscous, moves conveniently and

do not form any separation zones in the upstream region. Due to geometric constraints, the separation zone width is similar for both Newtonian and shear-thinning fluids.

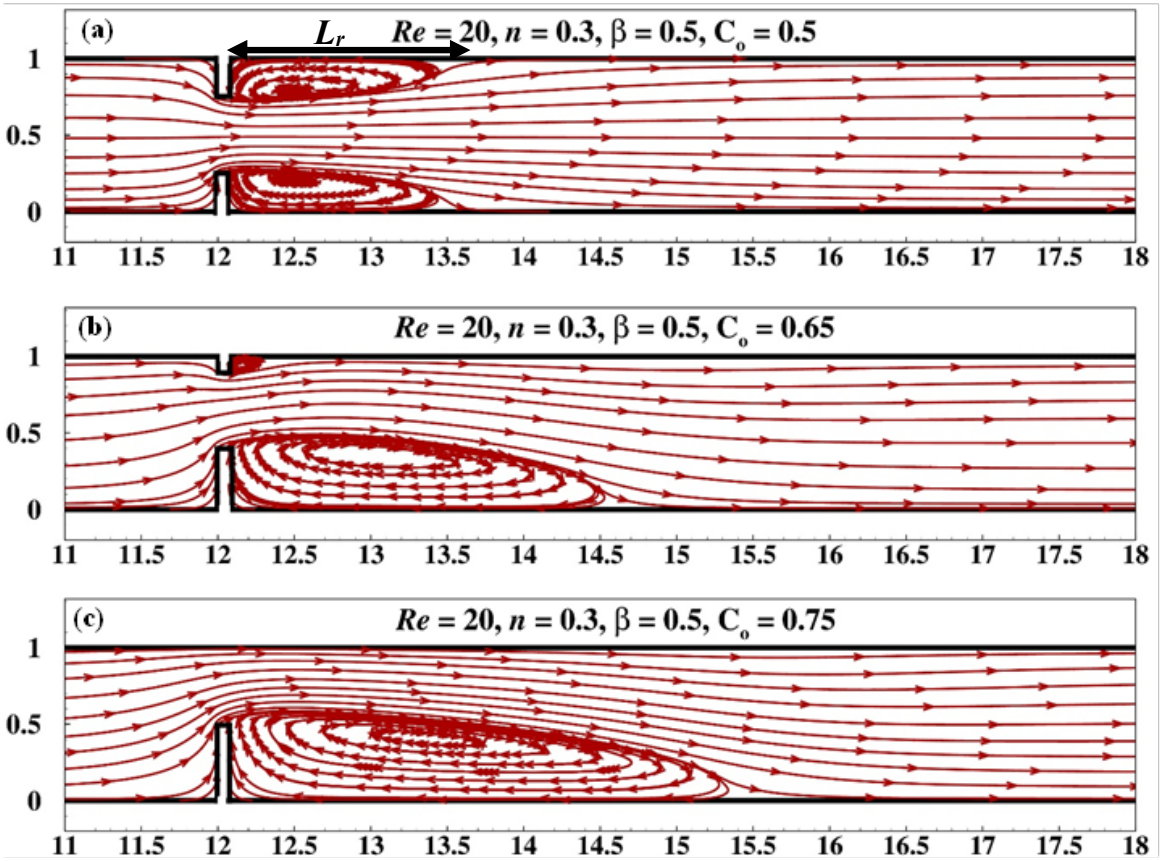

Fig. 2. Streamline patterns for three different lateral position of the orifice at $Re = 20$, $\beta = 0.5$ for highly shear-thinning fluids, $n = 0.3$.

4.2. Centreline Velocity Profile

Figure 4 represents the centreline velocity profile, U_c, for two lateral positions of the orifice in the channel as $C_o = 0.5$ and 0.65 at $Re = 20$, $\beta = 0.5$, and for three values of the power-law index as $n = 0.3$, 0.6 and 1.0 at Reynolds number, $Re = 20$ and aspect ratio, $\beta = 0.5$. A strong influence of the lateral positions of the location of the orifice can be observed in Figs. 4(a) and (b). Regardless of the location of orifice and constrictions in the channel, a sharp peak in the axial velocity profile, U_c has been noted in Figs. (a) and (b), due to the obstruction in the fluid field leading to the Bernoulli effect. Notably, it has also been observed that, in such figures, the fluid velocity has also been increased with a gradual increment in the power-law index due to the dominance of the viscous forces. In other words, the Newtonian fluid velocity is higher than the non-Newtonian fluids, as also reported in Ref. [18]. Importantly, it is interesting to note that as the location of the orifice approaches the upper wall of the channel, ~ 16% decrease in the maximum centreline fluid velocity has been observed between $C_o = 0.5$ and 0.65 at $Re = 20$, $\beta = 0.5$, see, Fig. 4(a) and (b). Such comparison with $C_o = 0.75$ further suppresses the velocity profile (the figure has not been included for the conciseness of the manuscript). Thus, suffice it to say here that a significant influence of the placement of the orifice location in the channel on the centreline velocity profile has been experienced.

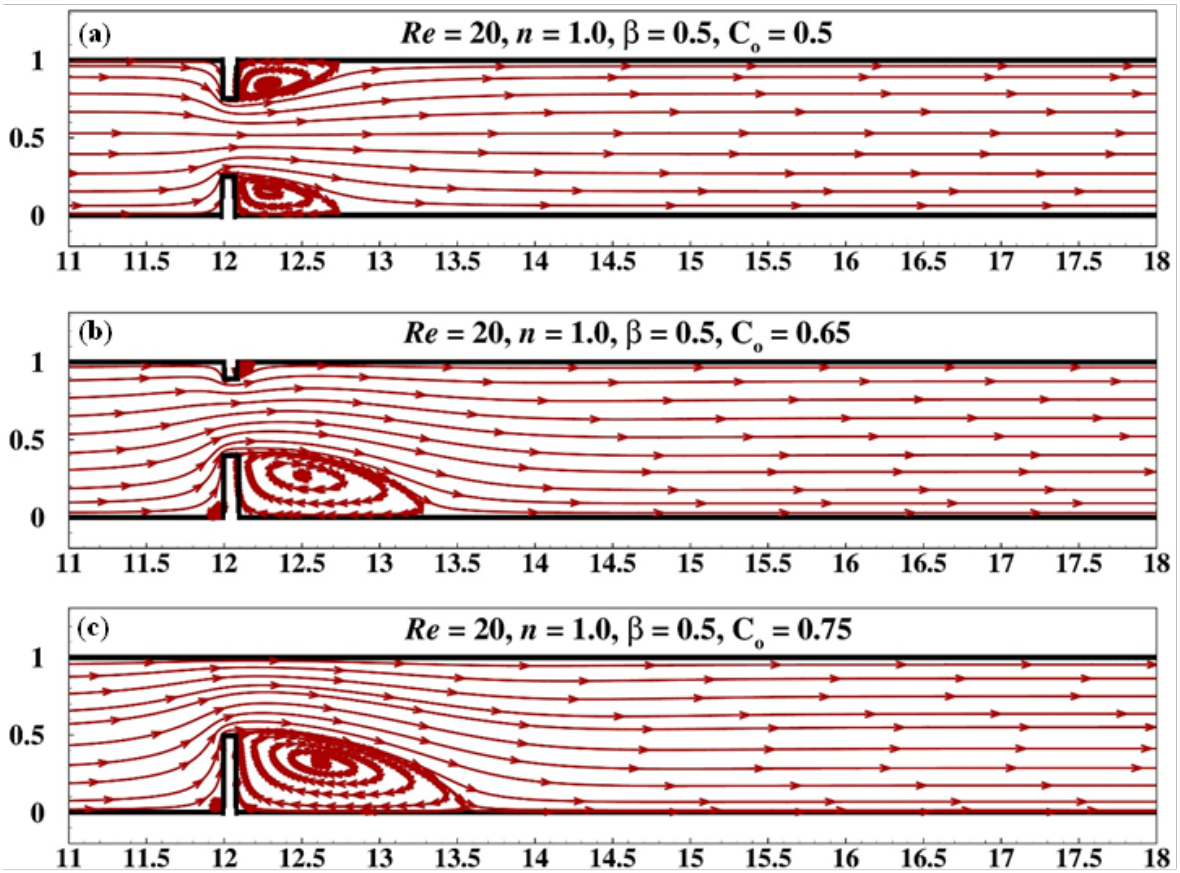

Fig. 3. Streamline patterns for three different lateral position of orifice at Re = 20, β = 0.5 for Newtonian fluids, n = 1.0.

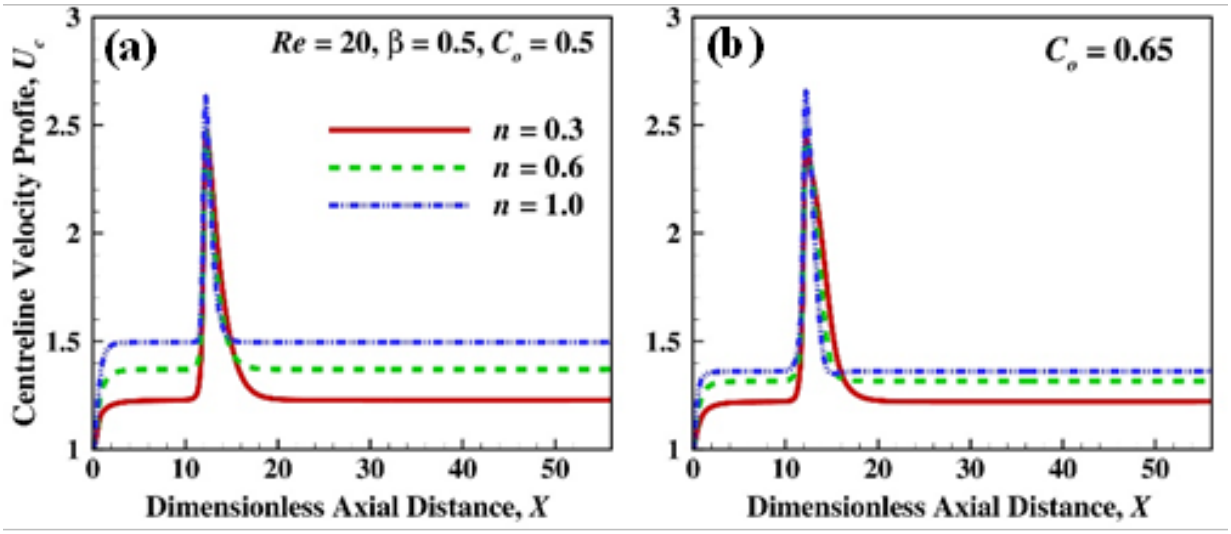

Fig. 4. Centreline velocity profile for three lateral positions of orifice in the channel at Re = 20 and β = 0.5 for (a) C_o = 0.5 (b) C_o = 0.65.

4.3. Lateral Velocity Profile

Figure 5 shows the lateral velocity profile, U_x, for two values of the orifice location as C_o = 0.5 (Fig. 5a) and 0.65 (Fig. 0.65 (Fig. 5b) at Re = 20, β = 0.5 and for three values of the power-law index as n = 0.3, 0.6 and 1.0. The velocity profiles profiles shown in Fig. 5 have been plotted at a particular axial location, i.e., X = 12.14 in the vicinity of the orifice. It is is essential to mention that the negative velocities have been noted in the lateral direction regardless of orifice location and power-law index values. Such negative velocities are the representation of the presence of the separation zones. The length in the lateral direction up to negative velocity can be called the width of the separation zones; see Fig. 5(a). Such length is seen to be longer for the lower values of the power-law index, i.e., 0.3, demonstrating the high degree of the shear-thinning of the fluid. In contrast, such length is shorter for the Newtonian fluids, n = 1.0. It is also important to mention herein that the switch in the velocity profile, regardless of orifice location and power-law index at Re = 20 and aspect ratio, β = 0.5, can be attributed to the conservation of momentum at the location. Fig. 4 shows the maximum centreline velocity for the highest power-law index values as n = 1.0, i.e., Newtonian fluid. Furthermore, a significant effect of the constraint's location in the fluid flow can be noted regarding the separation width. For instance, a symmetric flow separation zone can be seen in case of C_o = 0.5 (see Fig. 5a), while it is asymmetric in the case of C_o = 0.65 for a given power-law index, Reynolds number, and aspect ratio, Fig. 5(b). However, at the lower wall of the channel, the flow separation zone is seen to be longer as the orifice shifts from C_o = 0.5 to 0.75 (figure not shown).

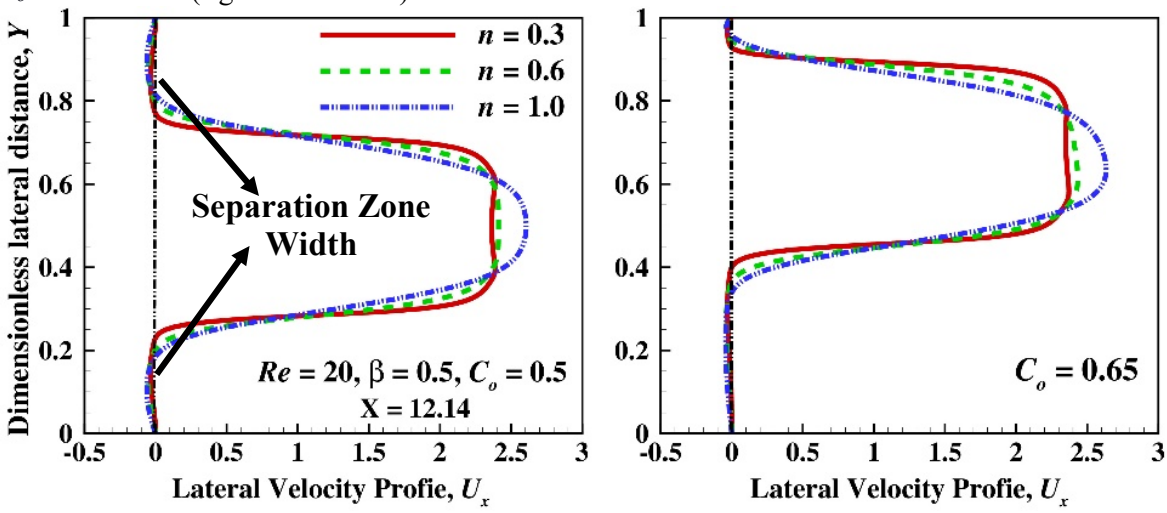

Fig. 5. Centreline velocity profile for three lateral positions of orifice in the channel at Re = 20 and β = 0.5 for (a) C_o = 0.5 (b) C_o = 0.65.

4.4. Discharge Coefficient, C_d

This section presents the variation in the discharge coefficient, C_d, of the orifice with the power-law index at Re = 20 and β = 0.5, for three different lateral positions of the orifice as C_o = 0.5, 0.65, and 0.75 in Fig. 6. The discharge coefficient for the non-Newtonian fluids has been calculated by the following equation, which has been derived from the basic Bernoulli equation:

Discharge coefficient through orifice, $$C_d = \sqrt{\frac{6(2n+1)^2}{(4n+3)(3n+2)}}\sqrt{\frac{1-\beta^2}{\beta^2}}\sqrt{\frac{1}{\Delta P^*}} \quad \text{..... (7)}$$

where, $\beta = H_o/H$, i.e., aspect ratio and $\Delta P^* = \left[2\Delta P/\left(\rho U_o^2\right)\right]$.

For a fixed, power-law index, n, Reynolds number, Re, and aspect ratio, β, the discharge coefficient is seen to be an increasing function of the shift of orifice location in the lateral direction. Such an effect is more pronounced 0.65 and 0.75. For instance, at $n = 0.6$, the difference between the discharge coefficient of $C_o = 0.65$ and 0.75 is ~17%. contrast, for $C_o = 0.5$ and 0.65, it is ~ 3.8%, see Fig. 6. Such observation can be attributed to the asymmetric flow field the case of $C_o = 0.65$ and 0.75. Moreover, for a given value of the orifice location, first, the discharge coefficient up to ~ $n \leq 0.6$, for $n > 0.6$, it decreases gradually till $n = 1$, see Fig. 6. This complex dependence of discharge coefficient the power-law index may be attributed to the interaction of non-linear terms of the momentum equation, i.e., the inertial term, which is scaled by U_o^2, and the viscous term, scaled by U_o^n, can be attributed to the complex interplay between the scaling factor of momentum equation. The complex interplay between the two scaling factors leads to the complex dependency of the discharge coefficient on a power-law index, as noted in Fig. 6.

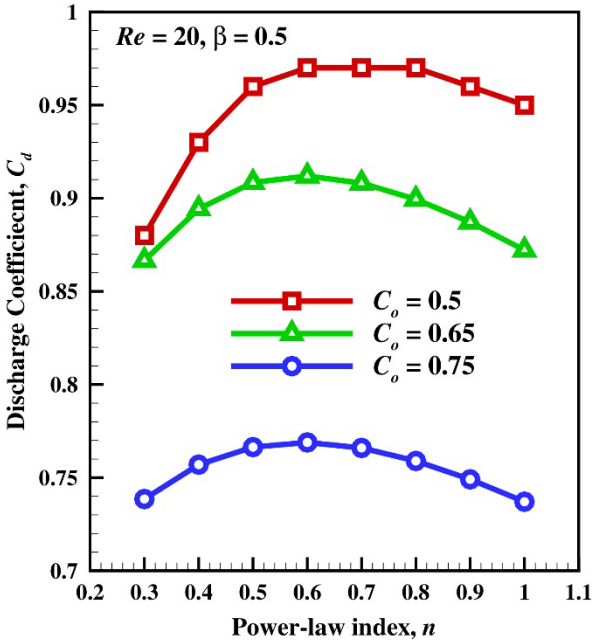

Fig. 6. Variation of Drag Coefficient with Power-law index at $Re = 20$ and $\beta = 0.5$ for three values of $C_o = 0.5$, 0.65 and 0.75.

5. Conclusions

The present work numerically investigates the influence of the shift of the orifice location in the lateral direction on the flow of non-Newtonian fluids, i.e., power-law fluids for a given Reynolds number (i.e., 20) and aspect ratio (i.e., 0.5). This work has been carried out for a wide range of power-law index ($n < 1$), including the Newtonian fluids, i.e., $n = 1.0$ and three lateral locations of the orifice as $C_o = 0.5$, 0.65, and 0.75. The new extensive results have been presented in the form of streamline patterns, velocity profiles, and discharge coefficients through the orifice. Results show a strong influence of orifice location (C_o) and fluid behaviour index (n) on the flow characteristics and discharge coefficient (C_d). In particular, symmetric and asymmetric separation zones have been noted close to channel walls in the vicinity of constriction region for a fix orifice location, regardless of the power-law index and Reynolds number. The maximum centreline velocity profile decreases with the shift of the orifice location close to the upper wall. The discharge coefficient also increases with an increase in C_o. A dramatic effect in terms of an increase and decrease in the discharge coefficient with power-law index (n) has been noted in this work, regardless of orifice location and Reynolds number in this work.

Nomenclature

C_d	discharge coefficient, dimensionless
H_o	width of the orifice, mm
H	channel width, m
L_{us}	length of the upstream region, m
L_{ds}	length of the downstream region, m
L_r	location of the reattachment point, dimensionless
$\dot{\gamma}$	rate of strain tensor, dimensionless
m	fluid consistency index, dimensionless
n	power-law index, dimensionless
N	unit normal vector, dimensionless
P_o	outlet pressure at the channel exit, Pa
ρ	density of fluids, Kg/m^3,
Re	Reynolds number based on the unobstructed channel width H, dimensionless
η	scalar viscosity function, dimensionless
t	orifice plate thickness, mm
τ	deviatoric stress tensor, dimensionless
β	H_o/H
u	axial velocity in x-direction, ms^{-1}
$\boldsymbol{U}$	velocity vector, dimensionless
U_o	average fluid velocity, ms^{-1}
U_x	axial velocity in x-direction [$= u/U_o$], dimensionless
U_y	axial velocity in y-direction [$= v/U_o$], dimensionless
v	axial velocity in y-direction, ms^{-1}
x, y	cartesian coordinates
X, Y	cartesian coordinates, dimensionless

References

[1] W.L. McCabe, J.C. Smith, and P. Harriott, *Unit operations of Chemical Engineering*. McGraw-Hill, International Editions, Singapore, 1993.

[2] E.F. Brater, H.W. King, J.E. Lindell and C.Y. Wei, *Handbook of Hydraulics*. McGraw-Hill, New York, NY, 1996.

[3] R.P. Chhabra, J.F. Richardson, *Non-Newtonian Fluids in the Process Industries: Fundamentals and Engineering Applications*. Butterworth-Heinemann, Oxford, UK, 1999.

[4] M. Reader-Harris, N. Barton and D. Hodges, "The effect of contaminated orifice plates on the discharge coefficient", Flow Meas. Instrum., 2012, vol. 25, pp. 2–7.

[5] M. Fossa and G. Guglielmini, "Pressure drop and void fraction profiles during horizontal flow through thin and thick orifices," Exp. Therm. Fluid Sci., 2002, vol. 26, pp. 513–523.

[6] D. S. Dugdale, "Viscous flow through a sharp-edged orifice". Int. J. Eng. Sci., 1997, vol. 35, pp. 725-729.

[7] B.N. Ntamba and V. Fester, "Pressure Losses and Limiting Reynolds Numbers for Non-Newtonian Fluids in Short Square-Edged Orifice Plates", J. Fluids Eng., 2012, vol.134, pp. 091204.

[8] M.R. Chowdhury and V.G. Fester, "Modeling pressure losses for Newtonian and non-Newtonian laminar and turbulent flow in long square edged orifices", Chem. Eng. Res. Des., 2012, vol. 90, pp. 863-869.

[9] M. Khahledi, R. Haldenwang, R. Chhabra, “Flow rate measurement of non-Newtonian fluids through sharp crested notches”, J. Hydraul. Eng., 2014, vol. 141, pp. 1-9.
[10] A. V. Rituraj, “Modelling the flow of non-Newtonian fluids through sharp orifices”, J. Fluids Eng. – ASME, 2018, vol. 140, pp. 1-6.
[11] M. Khahledi, R. Haldenwang, R. Chhabra and V. Fester, “Non-Newtonian fluid flow from bottom of tank using orifices of different shapes”, Chem. Eng. Res. Des., 2020, vol. 157, pp. 34-45.
[12] H.E. Merritt, *Hydraulic Control Systems.* John Wiley & Sons, Inc, 1967.
[13] V.S Bagade, P.M. Suryawanshi and S.M. Nalavade, “A review of multi-hole orifice plate”, Int. J. Res. Appl. Sci. Eng. Tech., 2019, vol. 7, no. 4, pp. 3197-3208.
[14] B. Teoman, A. Potanin, and P.M. Armenante, “The discharge of complex fluids through an orifice: A review”, Chem. Eng. Res. Des., 2022, vol. 179, pp. 346–36.
[15] S. Vemulapalli and S.K. Venkata, “Parametric analysis of orifice plates on measurement of flow: A review,” A in Shams Eng. J., 2022, vol. 13, no. 3, pp. 101639.
[16] A. Maurya, N. Tiwari, and R.P. Chhabra, “Effect of inclination angle on the forced convective flow of a power-law fluid in a 2-D planar branching channel,” Int. J. Heat Mass Transfer, 2019, vol. 134, pp. 768-783.
[17] A. Maurya, N. Tiwari, and R.P. Chhabra, “Controlling the flow and heat transfer characteristics of power-law fluids in T-junctions using a rotating cylinder,” Int. J. Therm. Sci., 2021, vol. 163, pp. 106854.
[18] F.-E. Moukhtari and B. Lecampion, “A semi-infinite hydraulic fracture driven by a shear-thinning fluid”, *J. Fluid Mech.*, vol. 838, pp. 573 – 605, 2018.